Nuclear Science and Techniques (2025) 36:229
https://doi.org/10.1007/s41365-025-01823-z

Dynamics of light nuclei produced in the massive transfer reactions

Zi-Han Wang[1] · Ya-Ling Zhang[2] · Zhao-Qing Feng[1]

Received: 30 April 2025 / Revised: 15 July 2025 / Accepted: 19 July 2025 / Published online: 29 September 2025

Abstract
Within the framework of the dinuclear system (DNS) model by implementing the cluster transfer into the dissipation process, we systematically investigated the energy spectra and the angular distribution of the pre-equilibrium clusters (n, p, d, t, ^{3}He, α, ^{6,7}Li, ^{8,9}Be) in the massive transfer reactions of ^{12}C+^{209}Bi, ^{14}N+^{159}Tb, ^{14}N+^{169}Tm, ^{14}N+^{181}Ta, ^{14}N+^{197}Au, ^{14}N+^{209}Bi, ^{58,64,72}Ni+^{198}Pt near the Coulomb barrier energies. It was found that the neutron emission is the most probable in comparison with the charged particles, and the α yields are comparable to the hydrogen isotopes in magnitude. Prequilibrium clusters are mainly produced from projectile-like and target-like fragments during the evolution of the dinuclear system. The kinetic energy spectra manifest a Boltzmann distribution, and the Coulomb potential influences the structure. The pre-equilibrium clusters follow the angular distribution of the multinucleon transfer fragments.

Keywords Pre-equilibrium cluster emission · Massive transfer reaction · Dinuclear system model

1 Introduction

The cluster structure in an atomic nucleus is a spatially located subsystem consisting of strongly related nucleons with much greater internal binding energy than external nucleons, which can be treated as a whole without considering its internal structure [1]. In 1968, Ikeda proposed that nuclear cluster states tend to occur in excited states near cluster threshold energy [2]. In some weakly bound nuclei, the cluster structure is more obvious, and the cluster structure is also ubiquitous in light nuclei; for example, the configuration of ^{6}Li is composed of a α particle and a deuteron, the 2α structure for ^{8}Be, 3α for ^{12}C, and 5 α for ^{20}Ne [3, 4]. The most convenient method to study the cluster structure inside a nucleus is to separate the cluster via pick-up or stripping reactions. A theoretical explanation of the pre-equilibrium reaction was initially developed using the exciton model. Semi-classical theories have been less successful in explaining the angular distribution of emitted particles. The Boltzmann master equation theory was mainly used to calculate the energy spectra of particles emitted during nucleon-induced reactions and heavy-ion reactions. Details can be found in the review paper [5]. However, the emission of pre-equilibrium clusters in transfer reactions around the Coulomb barrier is also an important physical problem. The emission of pre-equilibrium clusters is a complex process that is related not only to the cluster structure of the collision system but also to the dynamics of the reaction. In the treatment of nuclear structures, the cluster state is the overlap of the single-particle wave functions. In the nuclear reaction, the formation of a pre-equilibrium particle is different from the cluster emitted during the de-excitation of a composite nucleus, and a pre-equilibrium cluster is formed before the formation of the compound nucleus. Its emission continues until the formation of the composite nucleus, and the pre-equilibrium cluster may be emitted from any fragment during the reaction. Cluster emission provides important information for the study of single-particle states or multiparticle correlation of nuclei and is a powerful tool for nuclear spectroscopy [5]. Moreover, cluster emission in intermediate- and high-energy heavy-ion collisions is also

This work was supported by the National Natural Science Foundation of China (Nos. 12175072 and 12311540139).

✉ Ya-Ling Zhang
zhangyl@impcas.ac.cn

Zhao-Qing Feng
fengzhq@scut.edu.cn

[1] School of Physics and Optoelectronics, South China University of Technology, Guangzhou 510640, China

[2] State Key Laboratory of Heavy Ion Science and Technology, Institute of Modern Physics, Chinese Academy of Sciences, Lanzhou 730000, China

important for investigating nuclear fragmentation and little-bang nucleosynthesis [6–8].

Since multinucleon transfer (MNT) reactions and deep inelastic heavy-ion collisions were proposed in the 1970 s [9–11], a large number of experiments have been carried out to measure the double differential cross sections, angular distributions, and energy distributions of different reaction systems. However, it is worth noting that there has been relatively little experimental and theoretical research on pre-equilibrium cluster emissions in transfer reactions. In the 1980 s, scientists at RIKEN in Japan and IMP in China measured the pre-equilibrium cluster emission of the transfer reactions of ^{14}N+^{159}Tb, ^{169}Tm, ^{181}Ta, ^{197}Au, ^{209}Bi [12] and ^{12}C+^{209}Bi [13, 14], respectively. The angular distributions, kinetic energy spectra, and total production cross sections of the emitted particles were measured experimentally. As we all know, since the concept of superheavy stable island was proposed in the 1960 s, the synthesis of superheavy nuclei has become an important frontier in the field of nuclear physics. In the past few decades, 15 types of superheavy elements $Z = 104 \sim 118$ [15] have been artificially synthesized by hot fusion or cold fusion reactions. However, owing to the limitations of projectile-target materials and experimental conditions, it is difficult for the fusion evaporation reaction to reach the next period of the periodic table. With MNT reactions, many nuclei can be generated depending on the transfer channels, and with the development of separation and detection technology, the MNT reaction may be the most promising method for synthesizing unknown superheavy elements. This mechanism has been applied to the production of heavy and superheavy isotopes [16, 17].

The study of pre-equilibrium cluster emission in the MNT reaction is not only of great significance for understanding the cluster structure of the collision system but also for exploring the formation mechanism of the cluster, the kinetic information of the reaction process, and the nuclear astrophysical process. The high intensity accelerator facility (HIAF) built in Huizhou, China has a large energy range and a wide range of particle beams [18], which provides a good experimental platform for the study of nuclear cluster structures and cluster emission.

In this study, we systematically investigated the pre-equilibrium cluster emission in transfer reactions. The remainder of this paper is organized as follows. In Sect. 2, we provide a brief description of the DNS model for describing pre-equilibrium cluster production. In Sect. 3, the production cross sections, kinetic energy spectra, and angular distributions of the pre-equilibrium clusters are analyzed and discussed. A summary and perspective are presented in Sect. 4.

2 Brief description of the model

The dinuclear system (DNS) model was first proposed by Volkov [19] to describe deep inelastic heavy-ion collisions. For the first time, Adamian et al. applied the DNS model to fusion evaporation reactions in competition with the quasi-fission process to study the synthesis of superheavy nuclei [20–22]. The Lanzhou nuclear physics group has further developed the DNS model [23–26]; for example, they introduced the barrier distribution function method in the capture process, considered the effects of quasi-fission and fission in the fusion stage, used statistical evaporation theory, and the Bohr–Wheeler formula to calculate the survival probability of superheavy nuclei. The DNS model has been widely used to study the production cross section, quasi-fission, fusion dynamics, etc., in the synthesis of superheavy nuclei based on fusion evaporation (FE) reactions and multinucleon transfer (MNT) reactions [27–30].

Using the DNS model, we calculated the temporal evolution, kinetic energy spectra, and angular distributions of the pre-equilibrium clusters in the transfer reactions with incident energy near the Coulomb barrier. Compared to our previous work [31], we introduced the transfer of clusters in the master equation of the DNS model, and the Coulomb force was considered in the pre-equilibrium cluster emission process. A pre-equilibrium particle is formed before the formation of the compound nucleus, and its emission continues until the composite nucleus is formed. The cross section of pre-equilibrium particle emission (ν = n, p, d, t, ^{3}He, α, ^{6,7}Li and ^{8,9}Be) is defined as

$$\begin{aligned}\sigma_\nu(E_k,\theta,t) = \sum_{J=0}^{J_{\max}}\sum_{Z_1=Z_\nu}^{Z_{\max}}\sum_{N_1=N_\nu}^{N_{\max}} \pi\overline{\lambda}^2(2J+1)\int f(B) \\ \times T(E_{\text{c.m.}},J,B)P(Z_1,N_1,E_1(E_{\text{c.m.}},J),t,B) \\ \times P_\nu(Z_\nu,N_\nu,E_k)\mathrm{d}B.\end{aligned} \tag{1}$$

Here, E_k and θ are the kinetic energy and emission angle of the particles when they are ejected from projectile-like or target-like fragments, respectively, and t is the time of the reaction process. The reduced de Broglie wavelength $\overline{\lambda} = \hbar/\sqrt{2\mu E_{\text{c.m.}}}$, and $P(Z_1,N_1,E_1(E_{\text{c.m.}},J),t,B)$ denotes the realization probability of the DNS fragment (Z_1,N_1). $P_\nu(Z_\nu,N_\nu,E_k)$ is the emission probability of the pre-equilibrium particles. E_1 is the excitation energy for fragment (Z_1,N_1), which is associated with the center-of-mass energy $E_{\text{c.m.}}$ and the incident angular momentum J. The maximal angular momentum $J_{\max}$ is taken as the grazing collision of the two colliding nuclei. The DNS fragments (Z_1,N_1) range from light (Z_ν,N_ν) to the composite system $(Z_{\max},N_{\max})$, where $Z_{\max} = Z_{\text{T}} + Z_{\text{P}}$ and $N_{\max} = N_{\text{T}} + N_{\text{P}}$ are the total number of protons and neutrons, respectively.

2.1 The capture cross section of binary system overcoming the Coulomb barrier

In the capture stage, the collision system overcomes the Coulomb barrier, forming a composite system. The capture cross section is given by

$$\sigma_{\rm cap}(E_{\rm c.m.}) = \pi\bar{\lambda}^{-2}\sum_{J=0}^{J_{\max}}(2J+1)\times\int f(B)T(E_{\rm c.m.},J,B){\rm d}B, \quad (2)$$

where $T(E_{\rm c.m.},J,B)$ is the penetration probability that overcomes barrier B. For light and medium systems, $T(E_{\rm c.m.},J,B)$ is calculated using the well-known Hill–Wheeler formula [32, 33], $T(E_{\rm c.m.},J,B)=\left\{1+\exp\left\{-\frac{2\pi}{\hbar\omega(J)}\left[E_{\rm c.m.}-B-\frac{\hbar^2J(J+1)}{2\mu R_{\rm B}^2({\rm J})}\right]\right\}\right\}^{-1}$, where $\hbar\omega(J)$ is the width of the parabolic barrier at $R_{\rm B}(J)$. Owing to the effect of multidimensional quantum penetration, the Coulomb barrier appeared to be distributed. By introducing a barrier distribution function based on the original Hill–Wheeler formula [32], the penetration probability can be written as

$$T(E_{\rm c.m.},J)=\int f(B)\frac{1}{1+\exp\left\{-\frac{2\pi}{\hbar\omega(J)}\left[E_{\rm c.m.}-B-\frac{\hbar^2J(J+1)}{2\mu R_{\rm B}^2({\rm J})}\right]\right\}}{\rm d}B, \quad (3)$$

where $\hbar\omega(J)$ denotes the width of the parabolic barrier at $R_{\rm B}(J)$.

For the heavy systems, the collision system does not form a potential energy pocket after overcoming the Coulomb barrier, $T(E_{\rm c.m.},J)$ is calculated by the classic trajectory method,

$$T(E_{\rm c.m.},J)=\begin{cases}0, & E_{\rm c.m.}<B+J(J+1)\hbar^2/(2\mu R_{\rm C}^2),\\ 1, & E_{\rm c.m.}>B+J(J+1)\hbar^2/(2\mu R_{\rm C}^2).\end{cases} \quad (4)$$

The reduced mass is $\mu=m_{\rm n}A_{\rm P}A_{\rm T}/(A_{\rm P}+A_{\rm T})$, where $m_{\rm n}$, $A_{\rm P}$ and $A_{\rm T}$ are the nucleon mass and mass numbers of the projectile and target nuclei, respectively. $R_{\rm C}$ denotes the Coulomb radius and $R_{\rm C}=r_{0c}\times(A_{\rm P}^{1/3}+A_{\rm T}^{1/3})$ with $r_{0c}=1.4\sim1.5$ fm.

The barrier distribution function is Gaussian form [25, 33]

$$f(B)=\frac{1}{N}\exp[-((B-B_{\rm m})/\Delta)^2]. \quad (5)$$

The normalization constant satisfies $\int f(B){\rm d}B=1$. Quantities $B_{\rm m}$ and Δ are evaluated as $B_{\rm m}=(B_{\rm C}+B_{\rm S})/2$ and $\Delta=(B_{\rm C}-B_{\rm S})/2$, respectively. $B_{\rm C}$ is the Coulomb barrier in the waist-to-waist orientation, and $B_{\rm S}$ is the minimum barrier obtained by varying the quadrupole deformation of the colliding partners. Here, we consider $B_{\rm S}$ as the Coulomb barrier in the tip-to-tip orientation.

2.2 The nucleon and cluster transfer dynamics

In the nucleon transfer process, the distribution probability of DNS fragments is obtained by numerically solving a set of master equations [34]. Fragment (Z_1,N_1) has the proton number of Z_1, the neutron number of N_1, the internal excitation energy of E_1, and the quadrupole deformation β_1, and the time evolution equation of its distribution probability can be described as

$$\begin{aligned}\frac{{\rm d}P(Z_1,N_1,E_1,\beta_1,B,t)}{{\rm d}t}&=\sum_{Z_1'=Z_1\pm1}W^{\rm p}_{Z_1,N_1,\beta_1;Z_1',N_1,\beta_1'}(t)\\&\times[d_{Z_1,N_1}P(Z_1',N_1,E_1',\beta_1',B,t)-d_{Z_1',N_1}P(Z_1,N_1,E_1,\beta_1,B,t)]\\&+\sum_{N_1'=N_1\pm1}W^{\rm n}_{Z_1,N_1,\beta_1;Z_1,N_1',\beta_1'}(t)\\&\times[d_{Z_1,N_1}P(Z_1,N_1',E_1',\beta_1',B,t)-d_{Z_1,N_1'}P(Z_1,N_1,E_1,\beta_1,B,t)]\\&+\sum_{Z_1'=Z_1\pm1,N_1'=N_1\pm1}W^{\rm d}_{Z_1,N_1,\beta_1;Z_1,N_1',\beta_1'}(t)\\&\times[d_{Z_1,N_1}P(Z_1',N_1',E_1',\beta_1',B,t)-d_{Z_1',N_1'}P(Z_1,N_1,E_1,\beta_1,B,t)]\\&+\sum_{Z_1'=Z_1\pm1,N_1'=N_1\pm2}W^{\rm t}_{Z_1,N_1,\beta_1;Z_1,N_1',\beta_1'}(t)\\&\times[d_{Z_1,N_1}P(Z_1',N_1',E_1',\beta_1',B,t)-d_{Z_1',N_1'}P(Z_1,N_1,E_1,\beta_1,B,t)]\\&+\sum_{Z_1'=Z_1\pm2,N_1'=N_1\pm1}W^{^3{\rm He}}_{Z_1,N_1,\beta_1;Z_1,N_1',\beta_1'}(t)\\&\times[d_{Z_1,N_1}P(Z_1',N_1',E_1',\beta_1',B,t)-d_{Z_1',N_1'}P(Z_1,N_1,E_1,\beta_1,B,t)]\\&+\sum_{Z_1'=Z_1\pm2,N_1'=N_1\pm2}W^{\alpha}_{Z_1,N_1,\beta_1;Z_1,N_1',\beta_1'}(t)\\&\times[d_{Z_1,N_1}P(Z_1',N_1',E_1',\beta_1',B,t)-d_{Z_1',N_1'}P(Z_1,N_1,E_1,\beta_1,B,t)].\end{aligned} \quad (6)$$

In this equation, $W_{Z_1,N_1,\beta_1;Z_1',N_1',\beta_1'}$ is the mean transition probability from channels (Z_1,N_1,E_1,β_1) to $(Z_1',N_1',E_1',\beta_1')$. The quantities d_{Z_1,N_1} indicate the microscopic dimensions corresponding to the macroscopic state (Z_1,N_1,E_1,β_1). In this process, the transfer of nucleons or clusters satisfies the relationships $Z_1'=Z_1\pm Z_\nu$ and $N_1'=N_1\pm N_\nu$, which represent the transfer of a neutron, proton, deuteron, tritium, ^{3}He, α. Note that we ignored the quasi-fission of DNS and fission of heavy fragments in the dissipation process. The initial probabilities of the projectile and target nuclei are set as $P(Z_{\rm proj},N_{\rm proj},E_1=0,t=0)=P(Z_{\rm targ},N_{\rm targ},E_1=0,t=0)=0.5$. The nucleon transfer process satisfies the unitary condition, $\sum_{Z_1,N_1}P(Z_1,N_1,E_1,t)=1$.

Similar to the cascade transfer of nucleons [25], the transfer of clusters is also described by the single-particle Hamiltonian,

$$H(t) = H_0(t) + V(t). \tag{7}$$

Single-particle states are defined with respect to the centers of the interacting nuclei, and are assumed to be orthogonalized in the overlap region. Thus, annihilation and creation operators depend on the reaction time. The total single-particle energy is

$$H_0(t) = \sum_K \sum_{\nu_K} \varepsilon_{\nu_K}(t)\alpha^+_{\nu_K}(t)\alpha_{\nu_K}(t). \tag{8}$$

The interaction potential is

$$\begin{aligned} V(t) &= \sum_{K,K'} \sum_{\alpha_K,\beta_{K'}} u_{\alpha_K,\beta_{K'}}(t)\alpha^+_{\alpha_K}(t)\alpha_{\beta_{K'}}(t) \\ &= \sum_{K,K'} V_{K,K'}(t). \end{aligned} \tag{9}$$

The quantity $\varepsilon_{\nu K}$ represents the single-particle energies, and $u_{\alpha_K,\beta_{K'}}$ are the interaction matrix elements parameterized in the following form:

$$\begin{aligned} u_{\alpha_K,\beta'_K} &= U_{K,K'}(t) \\ &\times \left\{ \exp\left[-\frac{1}{2}\left(\frac{\varepsilon_{\alpha_K}(t) - \varepsilon_{\beta_K}(t)}{\Delta_{K,K'}(t)} \right)^2 \right] - \delta_{\alpha_K,\beta_{K'}} \right\}. \end{aligned} \tag{10}$$

Here, the calculations of $U_{K,K'}(t)$ and $\delta_{\alpha_K,\beta_{K'}}(t)$ are described in Ref. [35].

In the relaxation process of relative motion, the DNS is excited by the dissipation of the relative kinetic energy and angular momentum. The excited DNS opens a valence space in which valence nucleons have a symmetrical distribution around the Fermi surface. Only the particles in states within the valence space are actively excited and undergo transfer. The average of these quantities was calculated in the valence space as follows:

$$\Delta\varepsilon_K = \sqrt{\frac{4\varepsilon^*_K}{g_K}}, \quad \varepsilon^*_K = \varepsilon^* \frac{A_K}{A}, \quad g_K = A_K/12. \tag{11}$$

Here, ε^* is the local excitation energy of the DNS fragments, which provides the excitation energy for the mean transition probability. The number of valence states in the valence space is $N_K = g_K\Delta\varepsilon_K$, g_K is the single-particle density around the Fermi surface. The number of valence nucleons was $m_K = N_{K/2}$. The microscopic dimension for the fragment (Z_K, N_K) is evaluated by

$$d(m_1, m_2) = \binom{N_1}{m_1}\binom{N_2}{m_2}. \tag{12}$$

The mean transition probability is related with the local excitation energy and the transfer of nucleons or clusters, and it can be microscopically derived from the interaction potential in valence space as

$$\begin{aligned} W^{\nu}_{Z_1,N_1;Z'_1,N'_1} &= G_\nu \frac{\tau_{\rm mem}(Z_1,N_1,E_1;Z'_1,N'_1,E'_1)}{d_{Z_1,N_1}d_{Z'_1,N'_1}\hbar^2} \\ &\times \sum_{ii'} |\langle Z'_1,N'_1,E'_1,i'|V|Z_1,N_1,E_1, \text{ and } i\rangle|^2. \end{aligned} \tag{13}$$

G_ν represents the spin-isospin statistical factors, and we use the winger density approach to identify the particle types [36, 37], that is, $G_\nu = 1, 1, 3/8, 1/12, 1/12, 1/96$ for neutrons, protons, deuterons, tritium, ^{3}He, α, respectively. The cluster transition probability is related to the cluster formation probability with cluster structure, cluster potential, cluster binding energy, Mott effect, etc. Further improvements are needed in future work.

The memory time is connected with the internal excitation energy [38],

$$\tau_{\rm mem}(Z_1,N_1,E_1;Z'_1,N_1,E'_1) = \left[\frac{2\pi\hbar^2}{\sum_{KK'}\langle V_{KK}V^*_{KK'}\rangle} \right]^{1/2}, \tag{14}$$

$$\begin{aligned} \langle V_{KK}V^*_{KK'}\rangle &= \frac{1}{4}U^2_{KK'}g_K g'_K \Delta_{KK'}\Delta\varepsilon_K\Delta\varepsilon'_K \\ &\times \left[\Delta^2_{KK'} + \frac{1}{6}((\Delta\varepsilon_K)^2 + (\Delta\varepsilon'_K)^2) \right]^{-1/2}. \end{aligned} \tag{15}$$

The interaction matrix elements are calculated by

$$\begin{aligned} \sum_{ii'} |V_{ii'}|^2 &= \omega_{11}(i_1,i'_1) + \omega_{22}(i_1,i'_1) \\ &+ \omega_{12}(i_1,i'_1) + \omega_{21}(i_1,i'_1), \end{aligned} \tag{16}$$

in which

$$\omega_{KK'}(i,i'_1) = d_{Z_1,N_1}\langle V_{KK'}, V^*_{KK'}\rangle, \tag{17}$$

with the states $i(Z_1,N_1,E_1)$ and $i'(Z'_1,N'_1,E'_1)$.

In the relaxation process of relative motion, the DNS is excited by the dissipation of the relative kinetic energy. The local excitation energy is determined by the dissipation energy from the relative motion and the potential energy surface of the DNS [26, 28],

$$\varepsilon^*(t) = E_{\rm diss}(t) - \big(U(\{\alpha\}) - U(\{\alpha_{\rm EN}\})\big), \tag{18}$$

where $\alpha_{\rm EN} = Z_{\rm P}, N_{\rm P}, Z_{\rm T}, N_{\rm T}, J, R, \beta_{\rm P}, \beta_{\rm T}, \theta_{\rm P}, \theta_{\rm T}$ for the projectile-target system. The excitation energy of DNS fragment (Z_1,N_1) is $E_1 = \varepsilon^*(t = \tau_{\rm int})A_1/A$. $\tau_{\rm int}$ denotes the interaction time, which is associated with the reaction system and relative angular momentum, and can be obtained using the deflection function [39]. The energy dissipated into the DNS is

$$E_{\rm diss}(t) = E_{\rm c.m.} - B - \frac{\langle J(t)\rangle(\langle J(t)\rangle + 1)\hbar^2}{2\zeta_{\rm rel}} - \langle E_{\rm rad}(J,t)\rangle, \tag{19}$$

and the radial energy is

$$\langle E_{\rm rad}(J,t)\rangle = E_{\rm rad}(J,0)\exp(-t/\tau_{\rm r}), \tag{20}$$

where the relaxation time of the radial motion is $\tau_{\rm r} = 5\times10^{-22}$ s, and the initial radial energy is $E_{\rm rad}(J,0) = E_{\rm c.m.} - B - J_i(J_i+1)\hbar^2/(2\zeta_{\rm rel})$. The dissipation of the relative angular momentum is described by

$$\langle J(t)\rangle = J_{\rm st} + (J_i - J_{\rm st})\exp(-t/\tau_J). \tag{21}$$

The angular momentum at the sticking limit is $J_{\rm st} = J_i\zeta_{\rm rel}/\zeta_{\rm tot}$ and the relaxation time $\tau_J = 15\times10^{-22}$ s. $\zeta_{\rm rel}$ and $\zeta_{\rm tot}$ are the relative and total moments of inertia of DNS, respectively. The initial angular momentum is set to $J_i = J$ in Eq. (1). The relaxation times of the radial kinetic energy and angular momentum are associated with the friction coefficients in binary collisions. The values in this work were obtained from an empirical analysis of deeply inelastic heavy-ion collisions [39, 40].

The potential energy surface (PES) of the DNS is evaluated as

$$U(\{\alpha\}) = B(Z_1,N_1) + B(Z_2,N_2) - B(Z,N) + V(\{\alpha\}), \tag{22}$$

with the relationship of $Z_1 + Z_1 = Z$ and $N_1 + N_1 = N$ [41, 42]. The symbol $\{\alpha\}$ denotes the quantities $Z_1, N_1, Z_2, N_2, J, R, \beta_1, \beta_2, \theta_1, \theta_2$. In the calculation, the distance R between the centers of the two fragments was chosen to be the value at the touching configuration, in which DNS is assumed to be formed, and $R = r_0\times(A_{\rm P}^{1/3} + A_{\rm T}^{1/3})$ with $r_0 = 1.2 \sim 1.3$ fm. $B(Z_i,N_i)(i=1,2)$ and $B(Z,N)$ are the negative binding energies of fragment (Z_i,N_i) and compound nucleus (Z,N), respectively. β_i represents the quadrupole deformations of the two fragments in the ground state, and $\theta_i(i=1,2)$ denotes the angles between the collision orientations and symmetry axes of the deformed nuclei. The interaction potential between fragment (Z_1,N_1) and (Z_2,N_2) is derived from

$$V(\{\alpha\}) = V_{\rm C}(\{\alpha\}) + V_{\rm N}(\{\alpha\}) + V_{\rm def}(t), \tag{23}$$

where $V_{\rm C}$ is the Coulomb potential using the Wong formula [43], $V_{\rm N}$ is the nucleus–nucleus potential using the double folding potential [20], and $V_{\rm def}(t)$ denotes the deformation energy of the DNS at reaction time t,

$$V_{\rm def}(t) = \frac{1}{2}C_1(\beta_1 - \beta_{\rm T}'(t))^2 + \frac{1}{2}C_2(\beta_2 - \beta_{\rm P}'(t))^2. \tag{24}$$

The quantity $C_i(i=1,2)$ denotes the stiffness parameters of the nuclear surface, which are calculated using the liquid-drop model [44]. The detailed calculations of $V_{\rm def}(t)$ can be obtained from Ref. [45] and the references therein. Figure 1 shows the PES in the collisions of ^{14}N+^{209}Bi and ^{64}Ni+^{198}Pt. The zigzag lines are the driving potentials, which are estimated by the minimal PES values during the process of transferring nucleons. The incident point is denoted by the star symbol.

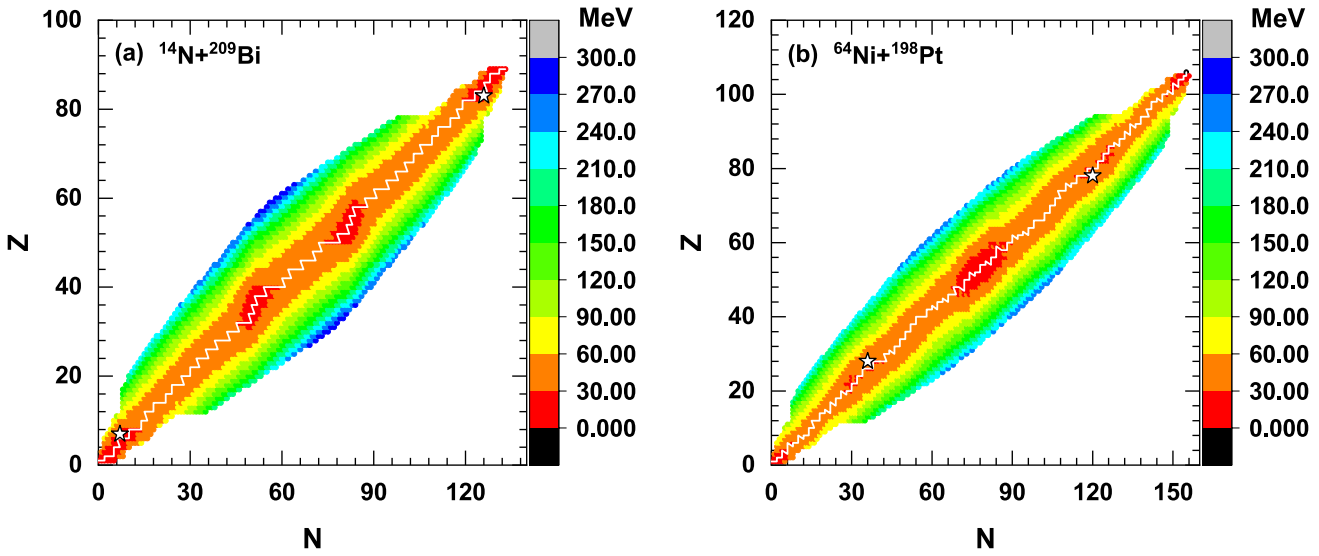

Fig. 1 (Color online) The potential energy surfaces in the reactions of **a** ^{14}N+^{209}Bi and **b** ^{64}Ni+^{198}Pt

2.3 The pre-equilibrium cluster emission

The emission probabilities of pre-equilibrium clusters with the kinetic energy E_k are calculated by the uncertainty principle within the time step $t \sim t + \triangle t$ via

$$P_\nu(Z_\nu, N_\nu, E_k) = \triangle t \Gamma_\nu / \hbar. \tag{25}$$

Here, the time step is set to $\triangle t = 0.5 \times 10^{-22}$ s for the reactions induced by ^{12}C and ^{14}N, but $\triangle t = 0.25 \times 10^{-22}$ s for the reactions induced by ^{58,64,72}Ni isotopes.

Based on the Weisskopf evaporation theory [46, 47], we have the particle decay widths as follows,

$$\Gamma_\nu(E^*, J) = (2s_\nu + 1)\frac{m_\nu}{\pi^2\hbar^2\rho(E^*, J)} \int_0^{E^*-B_\nu-E_{\rm rot}-V_{\rm c}} \times \varepsilon\rho(E^* - B_\nu - E_{\rm rot} - V_{\rm c} - \varepsilon, J)\sigma_{\rm inv}(\varepsilon){\rm d}\varepsilon, \tag{26}$$

where s_ν, m_ν and B_ν are the spin, mass, and binding energies of the evaporating particles, respectively.

The inverse cross section is given by

$$\sigma_{\rm inv} = \pi R_\nu^2 T(\nu), \tag{27}$$

with the radius of

$$R_\nu = 1.21\left[(A - A_\nu)^{1/3} + A_\nu^{1/3}\right]. \tag{28}$$

The penetration probability was set as $T(\nu) = 1$ for neutrons and $T(\nu) = [1 + \exp(2\pi(V_{\rm C}(\nu) - \varepsilon)/\hbar\omega)]^{-1}$ for charged particles with $\hbar\omega = 5$ MeV and 8 MeV for hydrogen isotopes and other charged particles, respectively. It should be mentioned that the local equilibrium of the DNS is assumed to be formed, and the excitation energy $E_i^* = \varepsilon_i^*$ for the i-th fragment is associated with the local excitation energy in the mass table [48].

The level density is calculated from the Fermi gas model as

$$\rho(E^*, J) = \frac{2J+1}{24\sqrt{2}\sigma^3 a^{1/4}(E^* - \delta)^{5/4}} \times \exp\left[2\sqrt{a(E^* - \delta)} - \frac{(J+1/2)^2}{2\sigma^2}\right], \tag{29}$$

where $\sigma^2 = 6\bar{m}^2\sqrt{a(E^* - \delta)}/\pi^2$ and $\bar{m} \approx 0.24A^{2/3}$. The pairing correction energy δ is set as $12/\sqrt{A}, 0$ and $-12/\sqrt{A}$ for even-even, even-odd, and odd-odd nuclei, respectively. The level density parameter is related to the shell correction energy $E_{\rm sh}(Z, N)$ and the excitation energy E^* of the nucleus as

$$a(E^*, Z, N) = \tilde{a}(A)[1 + E_{\rm sh}(Z, N)f(E^* - \Delta)/(E^* - \Delta)]. \tag{30}$$

The asymptotic Fermi gas value of the level density parameter at a high excitation energy is $\tilde{a}(A) = \alpha A + \beta A^{2/3} b_{\rm s}$, and the shell damping factor is given by $f(E^*) = 1 - \exp(-\gamma E^*)$ with $\gamma = \tilde{a}/(\epsilon A^{4/3})$. The parameters α, β, $b_{\rm s}$ and ϵ are taken to be 0.114, 0.098, 1 and 0.4, respectively [41, 42].

The kinetic energy of the pre-equilibrium particle is sampled using the Monte Carlo method within the energy range $\epsilon_\nu \in (0, E^* - B_\nu - E_{\rm rot} - V_{\rm C})$ and $E_k = \epsilon_\nu + V_{\rm C}$. Here, $V_{\rm C}$ represents the Coulomb force that the outgoing particles must overcome, and for neutrons, $V_{\rm C} = 0$. Watt spectrum is used for the neutron emission [49] and expressed as

$$\frac{{\rm d}N_{\rm n}}{{\rm d}\epsilon_{\rm n}} = C_{\rm n}\frac{\epsilon_{\rm n}^{1/2}}{T_{\rm w}^{3/2}}\exp\left(-\frac{\epsilon_{\rm n}}{T_{\rm w}}\right) \tag{31}$$

with $T_{\rm w} = 1.7 \pm 0.1$ MeV and a normalization constant $C_{\rm n}$. For the charged particles, the Boltzmann distribution is taken into account as

$$\frac{{\rm d}N_\nu}{{\rm d}E_k} = 8\pi\epsilon_\nu\left(\frac{m_\nu}{2\pi T_\nu}\right)^{1/2}\exp\left(-\frac{\epsilon_\nu}{T_\nu}\right), \tag{32}$$

where mass m_ν and local temperature $T_\nu = \sqrt{E^*/a}$, and $a = A/8$ is the level density parameter.

We use the deflection function method [39, 50] to calculate the angular distribution of the pre-equilibrium particles emitted from the DNS fragments as

$$\Theta(J_i) = \Theta_{\rm C}(J_i) + \Theta_{\rm N}(J_i). \tag{33}$$

The Coulomb deflection is given by the Rutherford function as

$$\Theta(J_i)_{\rm C} = 2\arctan\frac{Z_{\rm p}Z_{\rm t}e^2}{2E_{\rm c.m.}b} \tag{34}$$

with incident energy $E_{\rm c.m.}$ and impact parameter b. The nuclear deflection is calculated by

$$\Theta(J_i)_{\rm N} = -\beta\Theta_{\rm C}^{\rm gr}(J_i)\frac{J_i}{J_{\rm gr}}\left(\frac{\delta}{\beta}\right)^{J_i/J_{\rm gr}}. \tag{35}$$

Here, $\Theta_{\rm C}^{\rm gr}(J_i)$ is the Coulomb scattering angle at grazing angular momentum $J_{\rm gr} = 0.22R_{\rm int}[A_{\rm red}(E_{\rm c.m.} - V(R_{\rm int}))]^{1/2}$. J_i is the incident angular momentum, $A_{\rm red}$ is the reduced mass of the collision system, and $V(R_{\rm int})$ denotes the interaction potential, where $R_{\rm int}$ is the Coulomb radius. The parameters δ and β are parameterized by fitting the deep inelastic scattering in massive collisions as

$$\beta = \begin{cases} 75f(\eta) + 15 & \eta < 375 \\ 36\exp(-2.17 \times 10^{-3}\eta) & \eta \geq 375 \end{cases} \tag{36}$$

and

$$\delta = \begin{cases} 0.07f(\eta) + 0.11 & \eta < 375 \\ 0.117\exp(-1.34\times10^{-4}\eta) & \eta \geq 375 \end{cases} \quad (37)$$

with

$$f(\eta) = \left[1 + \exp\frac{\eta - 235}{32}\right]^{-1}. \quad (38)$$

The quantity $\eta = \frac{Z_1 Z_2 e^2}{\upsilon}$ is the Sommerfeld parameter and the relative velocity is calculated as $\upsilon = \frac{2}{A_{\rm red}}(E_{\rm c.m.} - V(R_{\rm int}))^{1/2}$. For the i−th DNS fragment, the emission angle is determined by

$$\Theta_i(J_i) = \Theta(J_i)\frac{\xi_i}{(\xi_1 + \xi_2)} \quad (39)$$

with the moment of inertia ξ_i for the i-th fragment.

3 Results and discussion

The pre-equilibrium cluster emission in the transfer reaction is very complicated and is not only related to the structure of the collision system, for example, the preformation factor, but also to the dynamic evolution of the reaction process, that is, the dissipation of relative motion and the coupling of internal degrees of freedom of the reaction system. The emission of pre-equilibrium cluster is a non-equilibrium process of time and space evolution, which is a powerful probe for deeply investigating the MNT reaction dynamics.

The temporal evolution of the emission probability of n, p, d, t, ^{3}He and α from the transfer reactions of ^{14}N + ^{159}Tb, ^{169}Tm, ^{181}Ta and ^{197}Au at $E_{\rm lab}$ = 115 MeV is shown in Fig. 2 and Fig. 3, respectively. The formation of the compound nucleus is of the order of a few hundred zeptoseconds, while the reaction time of the pre-equilibrium process is approximately several zeptoseconds. It can be seen from the figures that the emission of the pre-equilibrium cluster continues until the formation of the composite nucleus. At the beginning of the reaction, the emission probability of the pre-equilibrium cluster increased rapidly, reaching a maximum value at approximately $20\times10^{-22} \sim 40\times10^{-22}$ s, and then remained stable or decreased gradually. The emission probabilities of α and hydrogen isotopes are comparable, and the yields are approximately 3 ∼ 4 orders of magnitude lower than that of neutrons but much larger than that of ^{3}He. The local excitation energy of the DNS fragment increases with time, and the emitted clusters can remove part of the energy, which is conducive to the formation of a compound nucleus with a lower excitation energy. The total emission cross sections of the pre-equilibrium clusters can be obtained by counting the temporal evolution of the cluster yields. The total emission cross sections of the different pre-equilibrium particles are shown in Table 1. It is obvious that the α yields are comparable with the proton emission

Figure 4 shows the kinetic energy spectra of the light nuclei produced in the transfer reactions ^{14}N + ^{159}Tb, ^{169}Tm, ^{181}Ta at $E_{\rm lab}$ =115 MeV. It can be seen from the figure

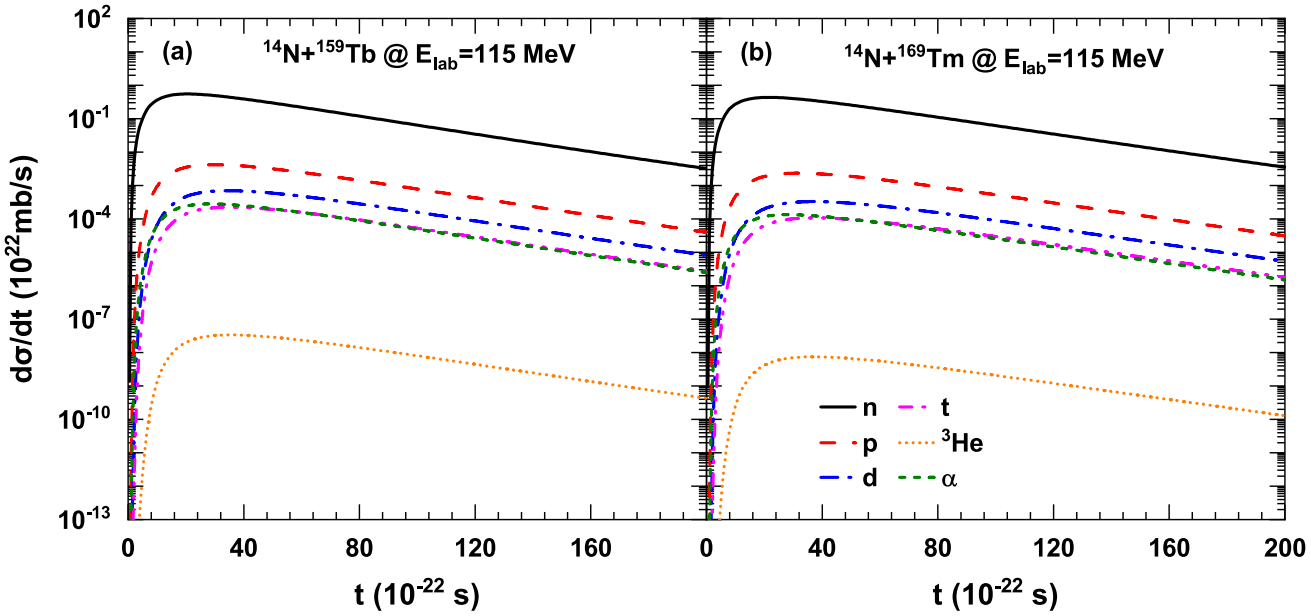

Fig. 2 Temporal evolution of the pre-equilibrium cluster emission in the reactions of **a** ^{14}N + ^{159}Tb and **b** ^{14}N + ^{169}Tm at the beam energy of 115 MeV

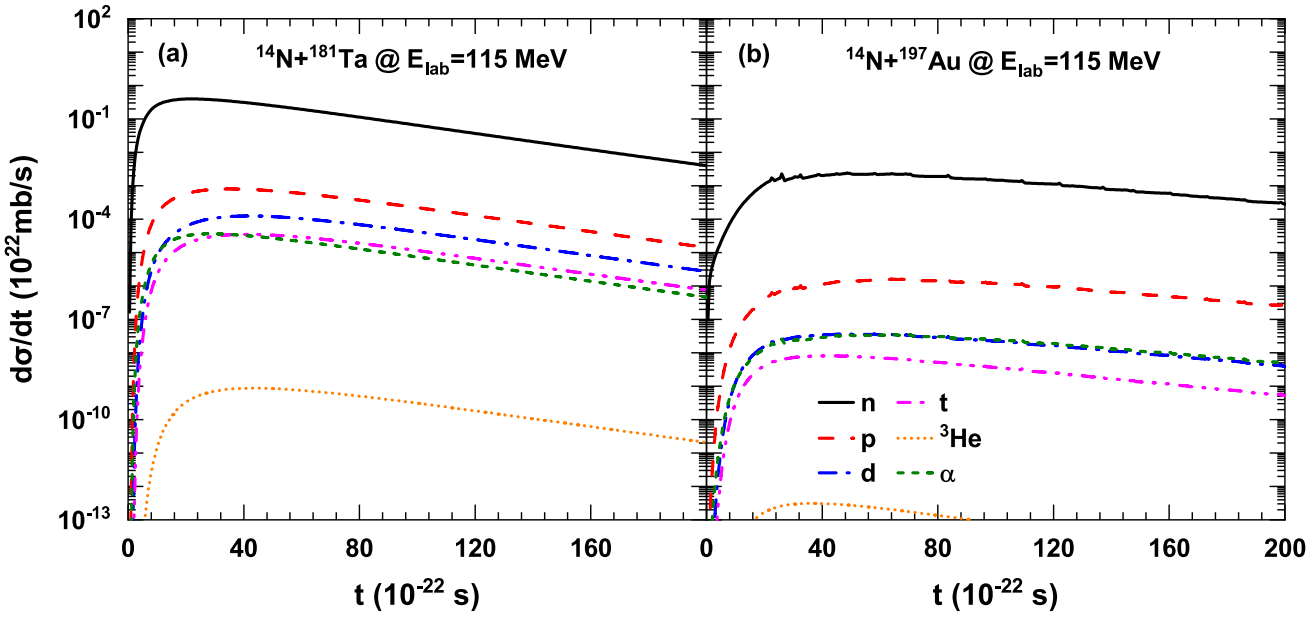

Fig. 3 The same as in Fig. 2, but for the collisions of ^{14}N on ^{181}Ta and ^{197}Au, respectively

Table 1 Production cross sections of neutron, proton, deuteron, triton, ^{3}He and α in the pre-equilibrium process of massive transfer reactions

Reaction system	E_{lab} (MeV)	σ_n (mb)	σ_p (mb)	σ_d (mb)	σ_t (mb)	$\sigma_{^3He}$ (mb)	σ_α (mb)
^{12}C+^{209}Bi	73	2.90×10^{-1}	2.58×10^{-6}	3.83×10^{-9}	4.06×10^{-8}	7.58×10^{-20}	4.54×10^{-6}
^{14}N+^{159}Tb	115	1.45×10^{-1}	1.29×10^{-6}	1.92×10^{-9}	2.03×10^{-8}	3.79×10^{-20}	2.27×10^{-6}
^{14}N+^{169}Tm	115	7.24×10^{-2}	6.46×10^{-7}	9.58×10^{-10}	1.02×10^{-8}	1.89×10^{-20}	1.13×10^{-6}
^{14}N+^{181}Ta	115	3.62×10^{-2}	3.23×10^{-7}	4.79×10^{-10}	5.08×10^{-9}	9.74×10^{-21}	5.67×10^{-7}
^{14}N+^{197}Au	115	1.81×10^{-2}	1.62×10^{-7}	2.40×10^{-10}	2.54×10^{-9}	4.74×10^{-21}	2.83×10^{-7}
^{14}N+^{209}Bi	115	9.05×10^{-3}	8.08×10^{-8}	1.20×10^{-10}	1.27×10^{-9}	2.37×10^{-9}	1.42×10^{-7}
^{58}Ni+^{198}Pt	170.2	1.11×10^{-4}	7.65×10^{-5}	7.16×10^{-8}	1.23×10^{-9}	4.30×10^{-10}	2.96×10^{-9}
^{58}Ni+^{198}Pt	185.6	2.78×10^{-5}	1.94×10^{-5}	1.79×10^{-8}	3.08×10^{-10}	1.07×10^{-10}	7.39×10^{-10}
^{64}Ni+^{198}Pt	181.4	6.94×10^{-6}	4.85×10^{-6}	4.47×10^{-9}	7.70×10^{-11}	2.69×10^{-11}	1.85×10^{-10}
^{72}Ni+^{198}Pt	176.0	1.74×10^{-6}	1.21×10^{-6}	1.12×10^{-9}	1.92×10^{-11}	6.72×10^{-12}	4.62×10^{-11}

that the kinetic energy spectra of the different reactions show a similar shape, presenting the Boltzmann distribution. The emission of neutrons was the most important factor. Compared with the previous work [31], we introduced Coulomb barrier correction in this study. Hydrogen isotopes have similar emission probabilities, owing to the same amount of charge, and the peak of their kinetic energy spectrum is approximately 10 MeV. Because α and ^{3}He are more charged, the kinetic energy spectra move in the direction of greater energy (i.e., to the right in the picture). In addition, we can see from Fig. 4 that the emission probability of α is approximately three to five orders of magnitude higher than ^{3}He, because the former has a lower separation energy and is more easily emitted from the DNS fragments. The calculation results above are consistent with experimental data [12, 14].

In Fig. 5, we show the kinetic energy spectra of the pre-equilibrium clusters (n, p, d, t, ^{3}He, α, ^{6,7}Li, ^{8,9}Be) in the transfer reactions induced by ^{12}C and ^{14}N to the same target nucleus ^{209}Bi. The kinetic energy spectra of these pre-equilibrium particles in the transfer reactions show the nuclear structure effect and the dynamic characteristics of the nuclear reaction. The available experimental data for the α emission from the HIRFL for the massive transfer reaction of ^{12}C+^{209}Bi [14] and from RIKEN for ^{14}N+^{209}Bi [12] are well reproduced with the DNS model. The excitation energy of DNS fragments, transition probability, binding energy, and separation energy of the transferred nucleons (clusters) affect the kinetic energy spectra. The

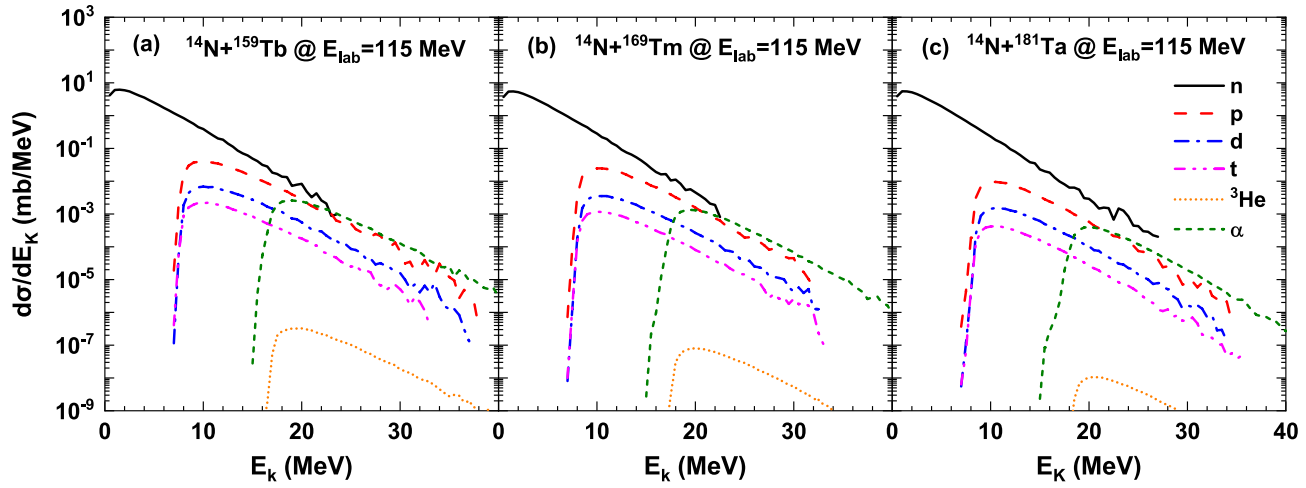

Fig. 4 (Color online) Kinetic energy spectra of the light nuclei produced in the reactions of **a** ^{14}N+^{159}Tb, **b** ^{169}Tm and **c** ^{181}Ta at E_{lab}=115 MeV, respectively

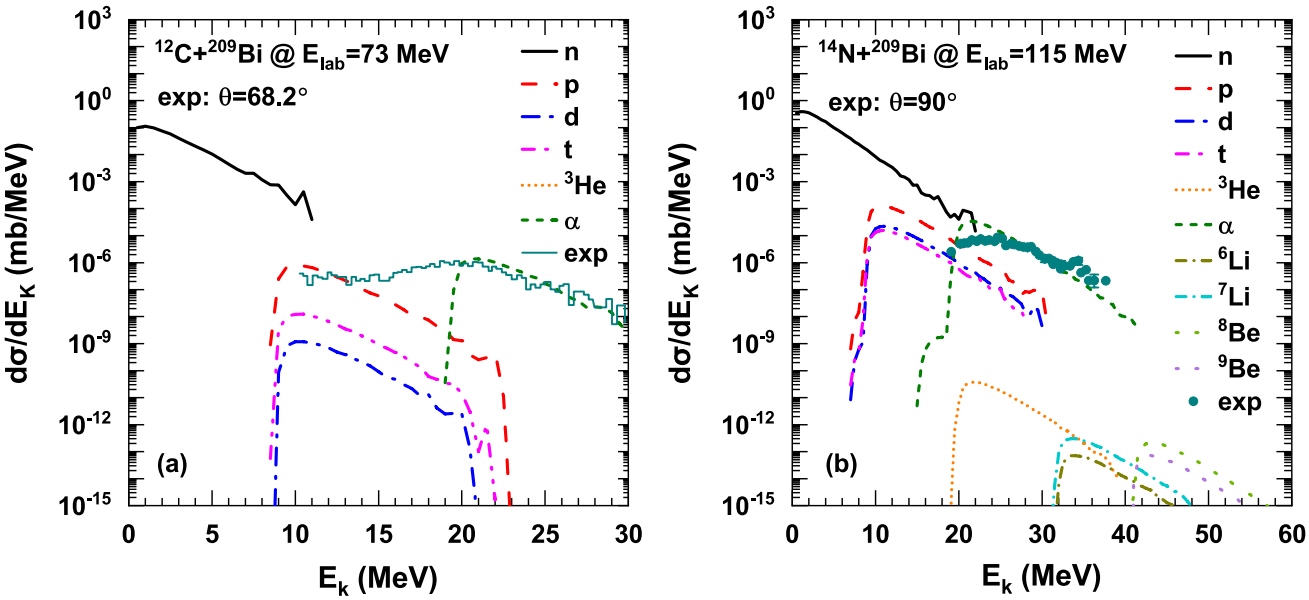

Fig. 5 Kinetic energy spectra of the pre-equilibrium clusters produced in collisions of **a** ^{12}C+^{209}Bi at E_{lab}=73 MeV and **b** ^{14}N+^{209}Bi at E_{lab}=115 MeV, respectively. The available experimental data (α particle) are shown for comparison from HIRFL for the reaction of ^{12}C+^{209}Bi [14] (left panel) and from RIKEN for ^{14}N+^{209}Bi [12] (right panel)

emission cross section of the pre-equilibrium cluster is mainly related to its formation probability and emission probability. In our calculation, it is assumed that the clusters already exist in the DNS; therefore, the emission cross sections of different clusters are mainly determined by the emission probabilities. The higher the charge of the emitted particle, the higher the Coulomb barrier. However, the larger the separation energy of the cluster, the smaller the decay width and the lower the emission probability. The kinetic energy spectra of the clusters are strongly related to the Coulomb barriers and excitation energies of the composite system.

The emission of the pre-equilibrium cluster is not only related to the reaction system, but also to the incident energy. Figure 6 shows a comparison of the time evolution and kinetic energy distribution of the transfer reaction, ^{58}Ni+^{198}Pt, at incident energies of 220 and 240 MeV. The left part of this figure shows the temporal evolution, and

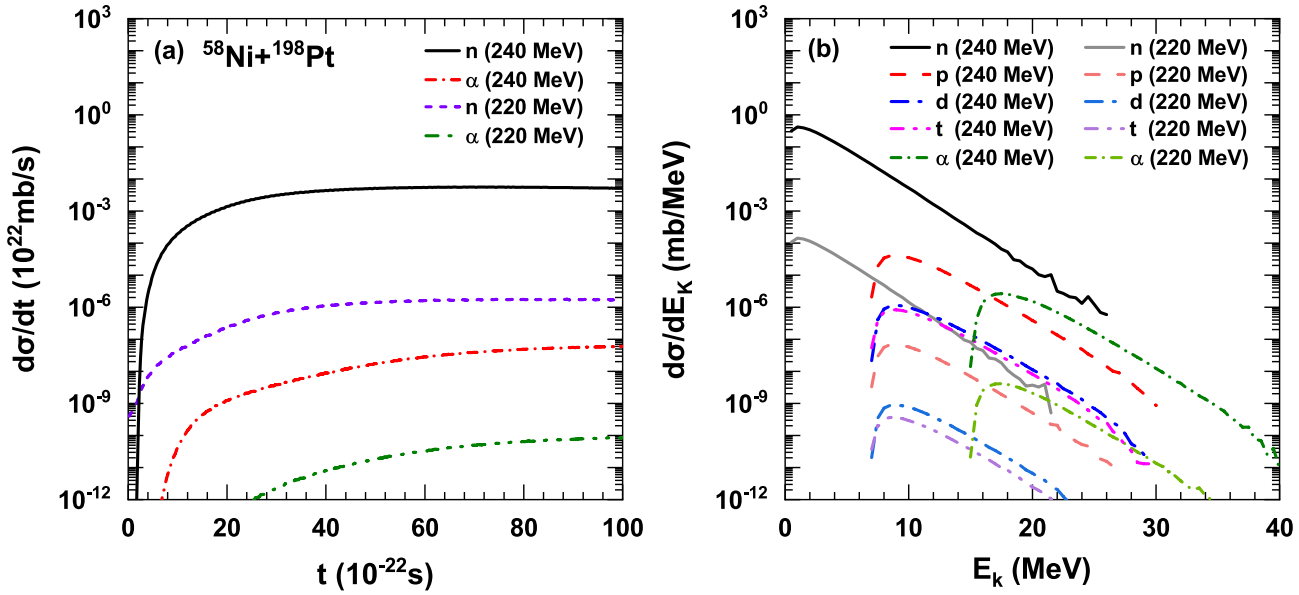

Fig. 6 **a** The temporal evolution and **b** kinetic energy spectra of the pre-equilibrium clusters produced in collisions of ^{58}Ni+^{198}Pt at $E_{c.m.}$=220 MeV and $E_{c.m.}$=240 MeV, respectively

the right part shows the kinetic energy spectra of the pre-equilibrium particles. The kinetic energy of the pre-equilibrium cluster is mainly determined by the local excitation energy of the projectile-like and target-like fragments, and a high local excitation energy is beneficial to cluster emission. We can see that the emission probability at $E_{c.m.}$ = 240 MeV is about 2 to 3 orders of magnitude higher than at $E_{c.m.}$ = 220 MeV, indicating that the emission probability of the pre-equilibrium clusters increased with the incident energy. In Fig. 7, we compare the transfer reactions of bombarding the target nucleus ^{198}Pt with heavier isotopes of Ni at $E_{c.m.}$ = 240 MeV, on the left is the kinetic energy spectra of the pre-equilibrium clusters emitted in the ^{64}Ni+^{198}Pt reaction, and on the right is the reaction of ^{72}Ni+^{198}Pt. Compared with the reaction system of ^{64}Ni+^{198}Pt, the reaction induced by ^{72}Ni seems to be more likely to emit neutrons, but the former is more likely to emit protons. In both reaction systems, the peak of the kinetic

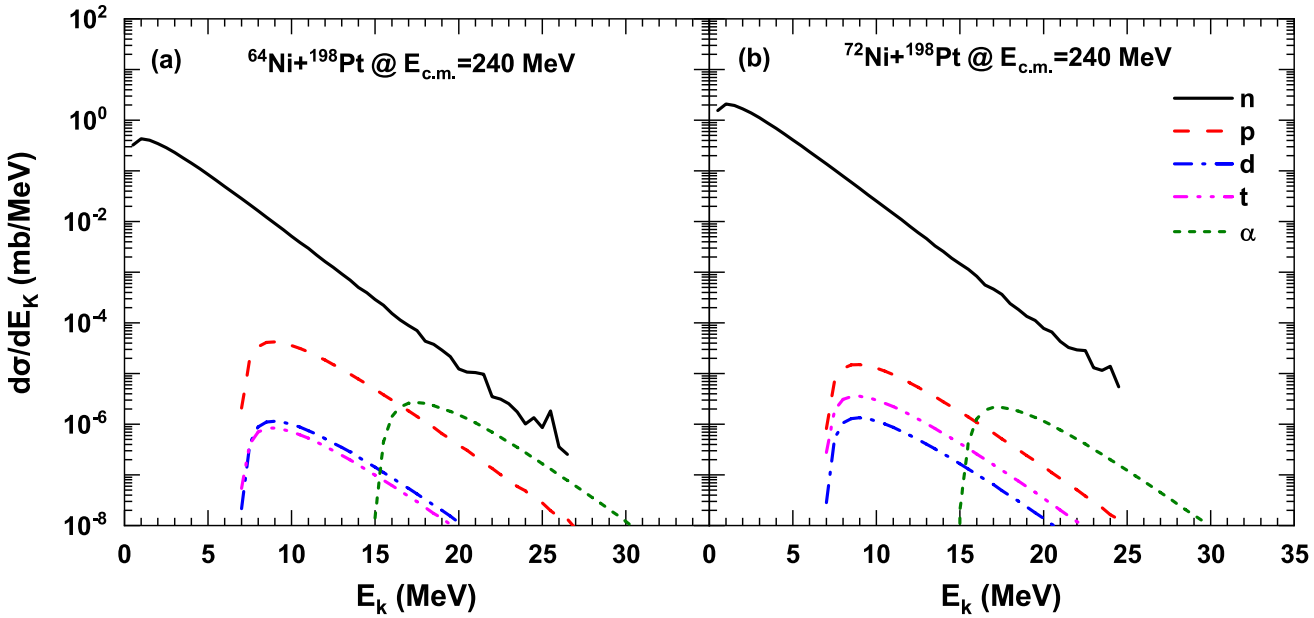

Fig. 7 Kinetic energy spectra of the pre-equilibrium clusters produced in collisions of ^{64,72}Ni+^{198}Pt at $E_{c.m.}$=240 MeV

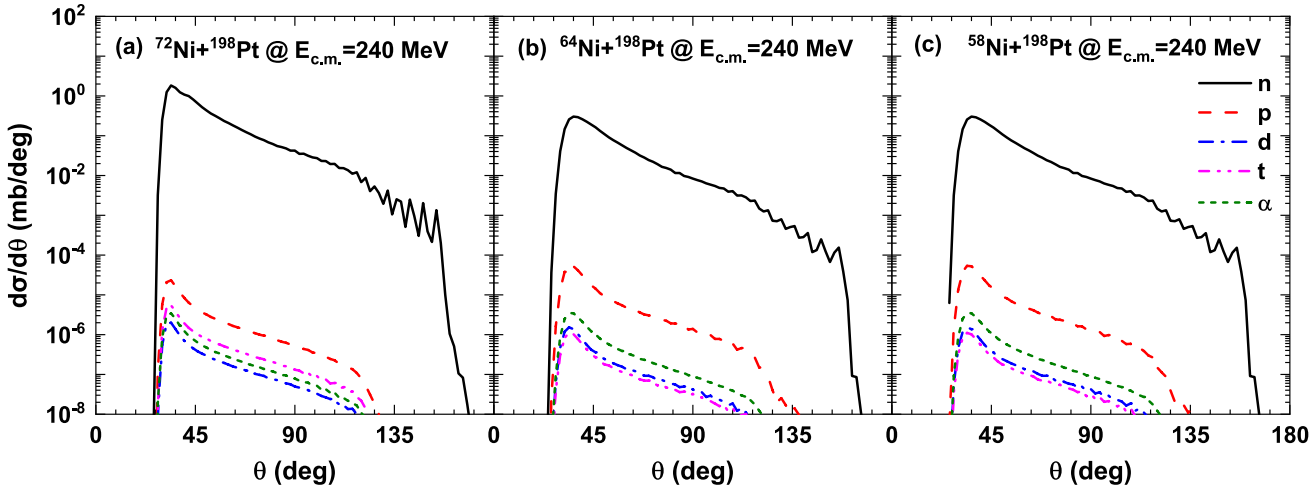

Fig. 8 Angular distributions of pre-equilibrium clusters in the reactions of ^{58,64,72}Ni+^{198}Pt at $E_{c.m.}$=240 MeV

energy spectra of the proton isotopes was approximately 9 MeV, while the peak of α kinetic energy spectra was approximately 17 MeV.

The particles emitted in the pre-equilibrium process and from the compound nucleus have different kinetic energies and angular distributions [51]. Direct particles primarily emit in the same direction as the incident particles and have similar energy to each other, while the particles of the compound process emit in all directions, in equal amounts forward and backward. Pre-equilibrium particles tend to be emitted forward and are generally more energetic than those from the composite nucleus. Shown in Fig. 8 is the angular distributions of the emitted pre-equilibrium clusters in ^{58,64,72}Ni+^{198}Pt at $E_{c.m.}$=240 MeV. The angular distribution was different for different reaction systems. For the same reaction system, the shapes of the angular distributions of different clusters are quite similar because different clusters may evaporate from the same excited DNS fragment. It can also be seen from the figure that the angular distributions of the pre-equilibrium particles are anisotropic, and their shapes show characteristics similar to of those the angular distributions of fragments in multinucleon transfer reactions [39, 50]. In the program calculation, we ignored the values for which the output was less than 1×10^{-10}. Under the three reaction systems, the angular distributions of the particles increased rapidly when the angle of the center of mass system was approximately 26° and reached a maximum value between 32° and 36°. There is a window of 32°–160° for the pre-equilibrium neutron emission. The study of the angular distribution of pre-equilibrium clusters in the transfer reaction is of great significance to the study of the angular distribution of the primary fragments in the MNT reaction and is helpful for the management of experimental measurements.

4 Conclusion

In summary, within the framework of the DNS model, we investigated the emission mechanism of the pre-equilibrium clusters in the massive transfer reactions near the Coulomb barrier energies, that is, the temporal evolution, kinetic energy spectra, and angular distributions of n, p, d, t, ^{3}He, α, ^{6,7}Li, ^{8,9}Be in collisions of ^{12}C+^{209}Bi, ^{14}N+^{159}Tb, ^{169}Tm, ^{181}Ta, ^{197}Au, ^{209}Bi, and ^{58,64,72}Ni+^{198}Pt. Cluster transfer and dynamic deformation are coupled to the relative dissipation of the angular momentum and motion energy in the DNS model. The emission of pre-equilibrium clusters strongly depends on the incident energy, separation energy, and Coulomb barrier from the primordial DNS fragments. The yields of hydrogen isotopes and α production have similar magnitudes but are more probable than those of heavy particles. The kinetic energy spectra manifest the difference of charged particles, that is, more kinetic energy for the α emission than the ones of protons. The pre-equilibrium clusters follow the MNT fragment emission on the angular distributions and are related to the correlation of the nucleons. The reaction mechanism is helpful for investigating the cluster structure of atomic nuclei and MNT fragment formation, that is, the yields, shell effect, and emission dynamics, which are being planned for future experiments at HIAF in Huizhou.

Author contributions All authors contributed to the study conception and design. Material preparation, data collection and analysis were performed by Zi-Han Wang, Ya-Ling Zhang and Zhao-Qing Feng. The first draft of the manuscript was written by Zi-Han Wang, and all authors commented on previous versions of the manuscript. All authors read and approved the final manuscript.

Declarations

Conflict of interest The authors declare that they have no competing interests.

References

1. Z.Y. Wei, Y.T. Zhu, Clustering property of nucleus. Nucl. Phys. Rev. **12**, 18–21 (1995). https://doi.org/10.11804/NuclPhysRev.12.03.018
2. K. Ikeda, N. Takigawa, H. Horiuchi, The systematic structure-change into the molecule-like structures in the self-conjugate 4n nuclei. Prog. Theor. Phys. Suppl. **E68**, 464–475 (1968). https://doi.org/10.1143/PTPS.E68.464
3. B. Zhou, Y. Funaki, H. Horiuchi et al., The 5α condensate state in ^{20}Ne. Nat. Commun. **14**, 8206 (2023). https://doi.org/10.1038/s41467-023-43816-9
4. T. Kawabata, The 5α condensate state in ^{20}Ne. Nucl. Sci. Tech. **35**, 35 (2024). https://doi.org/10.1007/s41365-024-01385-6
5. P.E. Hodgson, E. Běták, Cluster emission, transfer and capture in nuclear reactions. Phys. Rep. **374**, 1–89 (2003). https://doi.org/10.1016/S0370-1573(02)00268-5
6. H.G. Cheng, Z.Q. Feng, Novel approach to light-cluster production in heavy-ion collisions. Phys. Rev. C **109**, L021602 (2024). https://doi.org/10.1103/PhysRevC.109.L021602
7. R. Wang, Y.G. Ma, L.W. Chen et al., Kinetic approach of light-nuclei production in intermediate-energy heavy-ion collisions. Phys. Rev. C **108**, L031601 (2023). https://doi.org/10.1103/PhysRevC.108.L031601
8. K.J. Sun, R. Wang, C.M. Ko et al., Unveiling the dynamics of little-bang nucleosynthesis. Nat. Commun. **15**, 1074 (2024). https://doi.org/10.1038/s41467-024-45474-x
9. A.G. Artukh, V.V. Avdeichikov, G.F. Gridnev et al., New isotopes ^{29,30}Mg, ^{31,32,33}Al, ^{33,34,35,36}Si, ^{35,36,37,38}P, ^{39,40}S and ^{41,42}Cl produced in bombardment of a ^{232}Th target with ^{290} MeV ^{40}Ar ions. Nucl. Phys. A **176**, 284–288 (1971). https://doi.org/10.1016/0375-9474(71)90270-3
10. P.J. Buttle, L.J. Goldfarb, Systematics of nucleon transfer between heavy ions at low energies. Nucl. Phys. A **176**, 299–320 (1971). https://doi.org/10.1016/0375-9474(71)90272-7
11. A.G. Artukh, G.F. Gridnev, V.L. Mikheev et al., Transfer reactions in the interaction of ^{40}Ar with ^{232}Th. Nucl. Phys. A **215**, 91–108 (1973). https://doi.org/10.1016/0375-9474(73)90104-8
12. H. Utsunomiya, T. Nomura, T. Inamura et al., Preequilibrium α-particle emission in heavy-ion reactions. Nucl. Phys. A **334**, 127–143 (1980). https://doi.org/10.1016/0375-9474(80)90144-X
13. W.G. Shen, S.W. Xu, D.Y. Wang et al., α particle emitted in the reaction of ^{12}C on ^{209}Bi. Chin. Phys. C **1**, 70–78 (1977)
14. G.M. Jin, Y.X. Xie, Y.T. Zhu et al., Product cross sections for the reaction of ^{12}C with ^{209}Bi. Nucl. Phys. A **349**, 285–300 (1980). https://doi.org/10.1016/0375-9474(80)90455-8
15. M. Thoennessen, Discovery of isotopes of elements with $Z\geq100$. At. Data Nucl. Data Tables **99**, 312–344 (2013). https://doi.org/10.1016/j.adt.2012.03.003
16. H.M. Devaraja, A.V. Yeremin, S. Heinz et al., The study of multi-nucleon transfer reactions for synthesis of new heavy and superheavy nuclei. Phys. Part. Nucl. Lett. **19**, 693–716 (2022). https://doi.org/10.1134/S1547477122060085
17. T. Niwase, Y.X. Watanabe, Y. Hirayama et al., Discovery of new isotope ^{241}U and systematic high-precision atomic mass measurements of neutron-rich Pa-Pu nuclei produced via multinucleon transfer reactions. Phys. Rev. Lett. **130**, 132502 (2023). https://doi.org/10.1103/PhysRevLett.130.132502
18. J.C. Yang, J.W. Xia, G.Q. Xiao et al., High intensity heavy ion accelerator facility (HIAF) in China. Nucl. Instrum. Methods Phys. Res. Sect. B **317**, 263–265 (2013). https://doi.org/10.1016/j.nimb.2013.08.046
19. V. Volkov, Deep inelastic transfer reactions-the new type of reactions between complex nuclei. Phys. Rep. **44**, 93–157 (1978). https://doi.org/10.1016/0370-1573(78)90200-4
20. G. Adamian, N. Antonenko, R. Jolos et al., Effective nucleus-nucleus potential for calculation of potential energy of a dinuclear system. Int. J. Mod. Phys. E **05**, 191–216 (1996). https://doi.org/10.1142/S0218301396000098
21. G. Adamian, N. Antonenko, W. Scheid et al., Treatment of competition between complete fusion and quasifission in collisions of heavy nuclei. Nucl. Phys. A **627**, 361–378 (1997). https://doi.org/10.1016/S0375-9474(97)00605-2
22. G. Adamian, N. Antonenko, W. Scheid et al., Fusion cross sections for superheavy nuclei in the dinuclear system concept. Int. J. Mod. Phys. E **633**, 409–420 (1998). https://doi.org/10.1016/S0375-9474(98)00124-9
23. W. Li, N. Wang, J.F. Li et al., Fusion probability in heavy-ion collisions by a dinuclear-system model. Europhys. Lett. **64**, 750 (2003). https://doi.org/10.1209/epl/i2003-00622-0
24. Z.Q. Feng, G.M. Jin, F. Fu et al., Entrance channel dependence of production cross sections of superheavy nuclei in cold fusion reactions. Chin. Phys. Lett. **22**, 846 (2005). https://doi.org/10.1088/0256-307X/22/4/019
25. Z.Q. Feng, G.M. Jin, F. Fu et al., Production cross sections of superheavy nuclei based on dinuclear system model. Nucl. Phys. A **771**, 50–67 (2006). https://doi.org/10.1016/j.nuclphysa.2006.03.002
26. Z.Q. Feng, G.M. Jin, J.Q. Li et al., Formation of superheavy nuclei in cold fusion reactions. Phys. Rev. C **76**, 044606 (2007). https://doi.org/10.1103/PhysRevC.76.044606
27. Z.Q. Feng, G.M. Jin, J.Q. Li, Production of new superheavy Z=108–114 nuclei with ^{238}U, ^{244}Pu, and ^{248,250}Cm targets. Phys. Rev. C **80**, 057601 (2008). https://doi.org/10.1103/PhysRevC.80.057601
28. Z.Q. Feng, G.M. Jin, J.Q. Li et al., Production of heavy and superheavy nuclei in massive fusion reactions. Nucl. Phys. A **816**, 33–51 (2009). https://doi.org/10.1016/j.nuclphysa.2008.11.003
29. Z.Q. Feng, G.M. Jin, J.Q. Li, Influence of entrance channels on the formation of superheavy nuclei in massive fusion reactions. Nucl. Phys. A **836**, 82–90 (2010). https://doi.org/10.1016/j.nuclphysa.2010.01.244
30. F. Niu, P.H. Chen, Z.Q. Feng, Systematics on production of superheavy nuclei Z = 119–122 in fusion-evaporation reactions. Nucl. Sci. Tech. **32**, 103 (2021). https://doi.org/10.1007/s41365-021-00946-3
31. Z.Q. Feng, Preequilibrium cluster emission in massive transfer reactions near the coulomb barrier energy. Phys. Rev. C **107**, 054613 (2023). https://doi.org/10.1103/PhysRevC.107.054613
32. D.L. Hill, J.A. Wheeler, Nuclear constitution and the interpretation of fission phenomena. Phys. Rev. **89**, 1102–1145 (1953). https://doi.org/10.1103/PhysRev.89.1102
33. V.I. Zagrebaev, Y. Aritomo, M.G. Itkis et al., Synthesis of superheavy nuclei: How accurately can we describe it and calculate the cross sections? Phys. Rev. C **65**, 014607 (2001). https://doi.org/10.1103/PhysRevC.65.014607
34. Z.Q. Feng, Effect of cluster transfer on the production of neutron-rich nuclides near N=126 in multinucleon-transfer reactions. Phys. Rev. C **108**, L051601 (2023). https://doi.org/10.1103/PhysRevC.108.L051601
35. G.G. Adamian, N.V. Antonenko, W. Scheid, Characteristics of quasifission products within the dinuclear system model. Phys. Rev. C **68**, 034601 (2003). https://doi.org/10.1103/PhysRevC.68.034601

36. R. Mattiello, H. Sorge, H. Stöcker et al., Nuclear clusters as a probe for expansion flow in heavy ion reactions at (10–15)*A* GeV. Phys. Rev. C **55**, 1443–1454 (1997). https://doi.org/10.1103/PhysRevC.55.1443
37. Z.Q. Feng, Formation and dynamics of exotic hypernuclei in heavy-ion collisions. Phys. Rev. C **102**, 044604 (2022). https://doi.org/10.1103/PhysRevC.102.044604
38. C. Riedel, G. Wolschin, W. Nörenberg, Relaxation times in dissipative heavy-ion collisions. Z. Phys. A Atoms Nuclei **290**, 47–55 (1979). https://doi.org/10.1007/BF01408479
39. G. Wolschin, W. Nörenberg, Analysis of relaxation phenomena in heavy-ion collisions. Z. Phys. Atoms Nuclei **284**, 209–216 (1978). https://doi.org/10.1007/BF01411331
40. J.Q. Li, G. Wolschin, Distribution of the dissipated angular momentum in heavy-ion collisions. Phys. Rev. C **27**, 590–601 (1983). https://doi.org/10.1103/PhysRevC.27.590
41. Z.Q. Feng, G.M. Jin, J.Q. Li, Production of heavy isotopes in transfer reactions by collisions of ^{238}U+^{238}U. Phys. Rev. C **80**, 067601 (2009). https://doi.org/10.1103/PhysRevC.80.067601
42. Z.Q. Feng, Production of neutron-rich isotopes around $N = 126$ in multinucleon transfer reactions. Phys. Rev. C **95**, 024615 (2023). https://doi.org/10.1103/PhysRevC.95.024615
43. C.Y. Wong, Interaction barrier in charged-particle nuclear reactions. Phys. Rev. Lett. **31**, 766–769 (1973). https://doi.org/10.1103/PhysRevLett.31.766
44. W.D. Myers, W.J. Swiatecki, Nuclear masses and deformations. Nucl. Phys. **81**, 1–60 (1996). https://doi.org/10.1016/0029-5582(66)90639-0
45. P.H. Chen, Z.Q. Feng, C. Geng et al., Production of neutron-rich actinide isotopes in isobaric collisions via multinucleon transfer reactions. Nucl. Sci. Tech. **34**, 160 (2023). https://doi.org/10.1007/s41365-023-01314-z
46. V. Weisskopf, Statistics and nuclear reactions. Phys. Rev. **52**, 295–303 (1937). https://doi.org/10.1103/PhysRev.52.295
47. P.H. Chen, Z.Q. Feng, J.Q. Li et al., A statistical approach to describe highly excited heavy and superheavy nuclei. Chin. Phys. C **40**, 091002 (2016). https://doi.org/10.1088/1674-1137/40/9/091002
48. P. Möller, J.R. Nix, W.D. Myers et al., Nuclear ground-state masses and deformations. At. Data Nucl. Data Tables **59**, 185–381 (1995). https://doi.org/10.1006/adnd.1995.1002
49. H. Rossner, D.J. Hinde, J.R. Leigh et al., Influence of pre-fission particle emission on fragment angular distributions studied for ^{208}Pb(^{16}O,f). Phys. Rev. C **45**, 719–725 (1992). https://doi.org/10.1103/PhysRevC.45.719
50. C. Peng, Z.Q. Feng, Production of neutron-rich heavy nuclei around $N = 162$ in multinucleon transfer reactions. Eur. Phys. J. A **58**, 162 (2022). https://doi.org/10.1140/epja/s10050-022-00819-2
51. P.E. Hodgson, Pre-equilibrium processes in nuclear reactions. Nature **292**, 671–672 (1981). https://doi.org/10.1038/292671a0